glacies

MDPI

Article

Snow Surface Roughness at a Ski Resort During Melt

Steven R. Fassnacht [1,2,3,*], Javier Herrero [4] and Jessica E. Sanow [1]

[1] ESS-Watershed Science, Colorado State University, Fort Collins, CO 80523-1476, USA
[2] Cooperative Institute for Research into the Atmosphere, Colorado State University, Fort Collins, CO 80523-1375, USA
[3] Instituto Geológico y Minero de España, Ronda, 18001 Granada, Spain
[4] Modelling Nature, Department of Ecology, University of Granada, Beiro, 18071 Granada, Spain
* Correspondence: steven.fassnacht@colostate.edu; Tel.: +1-970-491-5454

Abstract

When snow is present, the snow surface is the interface between the atmosphere and the Earth's surface. The snowpack energy balance is dictated in part by snow surface roughness, which can be quite dynamic. At the Sierra Nevada ski resort in Spain, we measured several snow surface forms: natural, with the presence of dust, with the presence of sun cups, and groomed snow (tracked and between tracks). The snow surface was assessed in 2-dimensions from snow roughness boards and in 3-dimensions from iPad surface scanning to measure across resolutions. Both data collection methods yielded similar roughness estimates via random roughness (RR) and variogram analysis (scale break, SB, and fractal dimension, D) for each distinct surface, yet the roughness differences between the surfaces were substantial. The geometry-based aerodynamic roughness length (z_0) was computed for the iPad-scanned surfaces, yielding an order-of-magnitude variability in z_0. This produced an order-of-magnitude difference in modelled sublimation. This work can inform snow management at ski areas and reflects some of the snow-surface conditions encountered in a natural snowpack.

Keywords: snow surface; random roughness; variograms; scale break; fractal dimension; aerodynamic roughness length; z_0; sublimation

1. Introduction

Snow is the great equalizer [1]. As snow accumulates and covers the ground, the characteristics of the snow surface change [2], typically becoming smoother [3]. The snow surface varies substantially over the winter [4–6], often increases during melt [3,6,7], such as with the development of sun cups [8] (Figure 1), that can be enhanced by the presence of dust (Figure 1) [5,9].

The surface of the snowpack is the interface between the atmosphere and the earth when snow is present [10–12]. As such, this interface dictates the energy balance of the snowpack [13,14], in particular the latent heat flux and the sensible heat flux [15,16]. The surface can be defined by a variety of metrics [17]; the aerodynamic roughness length (z_0) is a component of these heat fluxes. However, most models assume that the snow surface is static and that z_0 is constant for snow [18].

At the sub-meter scale, snow surface roughness influences albedo [19]. The roughness occurs across a variety of scales [7,20]. Understanding the snow surface roughness is relevant for remote sensing of the snowpack [20]. At ski areas, grooming provides a smoother snow surface (Figure 1) [21]. Modelling of the snowpack for a ski resort is

Academic Editor: Ulrich Kamp

Received: 27 November 2025
Revised: 25 February 2026
Accepted: 2 March 2026
Published: 5 March 2026

challenging due to the snow management strategies [22]. Here, we argue that an additional challenge arises from the spatial variability of snow surface roughness. Thus, we asked the following questions: (1) How does the snow surface roughness vary at a ski area? and (2) what are the implications of the spatial variation on snowpack sublimation modelling? This examination uses several roughness metrics that have been applied across several scales of snow surface data [23], including z_0, to compare different surfaces seen at a ski resort. The latter metric is used in a sensitivity analysis for simple sublimation modelling.

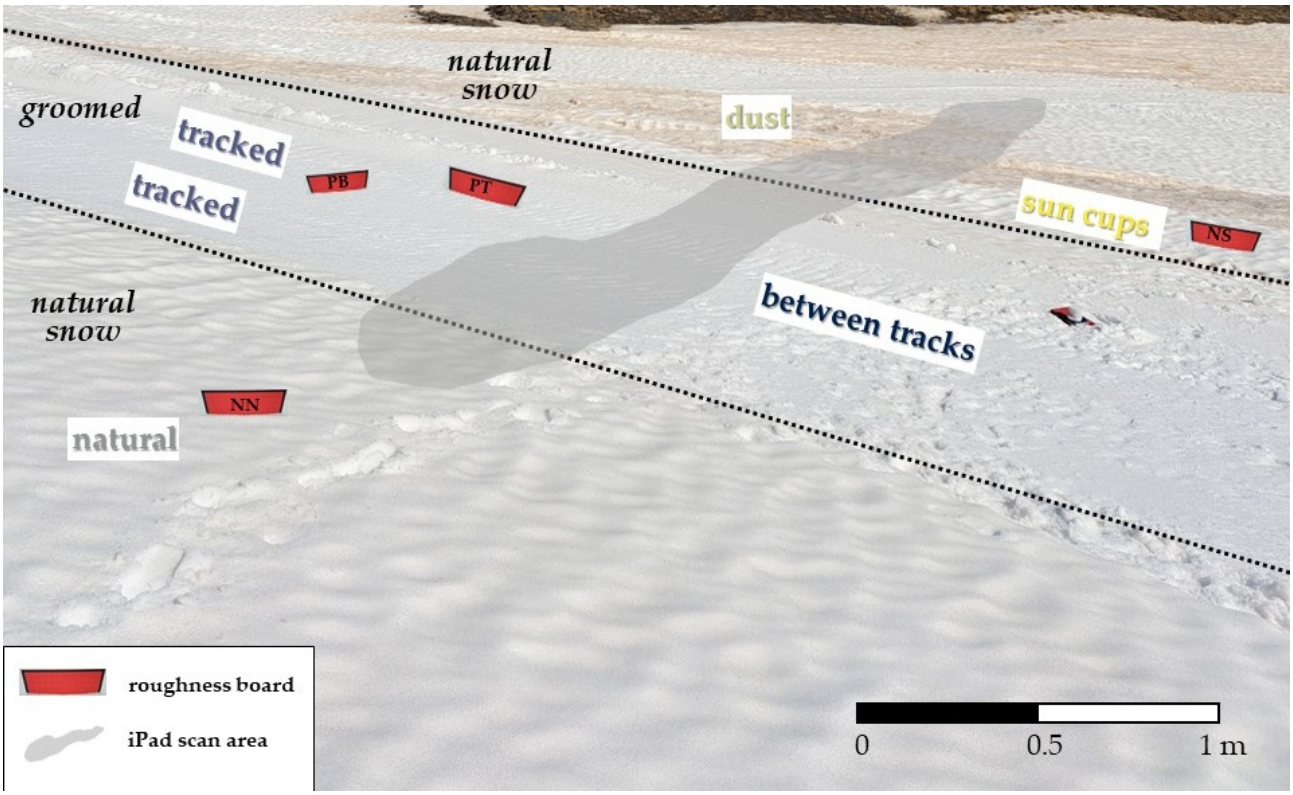

Figure 1. Photograph of the study area illustrating sun cups, groomed (tracked and between tracks or untracked), and dust at the surface (taken by Steven Fassnacht).

2. Study Site

In Spain, most areas with continuous seasonal snow cover lie above treeline [24,25]. Snow dominates the Spanish alpine environment (Figure 2a) [26], especially in the Sierra Nevada (Figure 2b) [27]. Snow is an important resource in the Spanish Sierra Nevada [28] for ski tourism [29], water resources [30], and for sustaining endemic fauna and flora [31,32], which make this area a biodiversity hotspot [33]. However, assessing the amount of snowfall is difficult [34]. Sublimation and melt-evaporation [35] reduces the water storage and further increases uncertainty [36].

To evaluate the uncertainty of sublimation, we collected data near the city of Granada (Figure 2a), in the northwestern Sierra Nevada (Figure 2b). Specifically, data were collected to the west of the top of the Telecabina Al-Andalus (Andalucian Gondola) (Figure 2c). This area, known as Borreguiles, is at an elevation of 2700 metres. Data were collected on 19 April 2024.

Figure 2. Location map (**a**) Spain, (**b**) Sierra Nevada Ski Resort, and (**c**) field site (37.0717° North latitude and 3.3946° West longitude). The black box is the greater study area and is 100 m wide by 200 m high. Maps from Google Maps and as such local labels are present, specifically the Parque Nacional de Sierra Nevada (Sierra Nevada National Park) located around the ski area, Cauchiles Glacier (Ventisquero de Cauchiles), the top of the gondola (denoted as Estacion de esqui Sierra Nevada or Sierra Nevada ski resort), and the local highest point (Pico Veleta).

3. Methods

3.1. Surface Mapping

We measured both the groomed snow surface, or piste [37], and the ungroomed (or natural) snow surface, also known as off-piste [38], at two spatial resolutions (0.2 mm and 1 cm) to estimate snow roughness (Figure 1). For the groomed surface, measurements included both the compacted tracks left by the grooming machine and the flatter sections between them (Figure 1). The ungroomed snow surface included natural snow with small undulations, sun cups, and dust at the surface (Figure 1 and Table 1). Roughness boards were used as a two-dimensional representation of fine details (sub-millimetre resolution) in the snowpack (Figure 3) while iPad surface scanning was used for a more coarse (centimetre resolution) three-dimensional surface geometry of the snow surface and Table 2. The latter were used to determine the sensitivity of snow surface roughness to sublimation modelling.

Table 1. Characteristics of the snow surfaces evaluated. The surface code presents groomed (P for piste) and natural (N). With P, the second letter T represents the tracked surface, and B is between tracks. With N, N is the natural surface, S is for sun cups, and D is for dust-on-snow. These surfaces are labelled in (Figure 1). N/A represents where data were not collected.

Surface Form	Code	Roughness Board	iPad Scanning
groomed/piste	PT	parallel to track	on groomer track
	PB	perpendicular to/ between track	between groomer tracks
natural	NN	natural	N/A
	NS	sun cups	sun cups
	ND	N/A	dust on snow

Table 2. Characteristics of the roughness boards and iPad scanning data.

Surface Characteristics	Roughness Board	iPad Scanning
dimensions	2-D	3-D
extent	0.6 m	0.8 m × 1.6 m
resolution	0.2 mm	1 cm

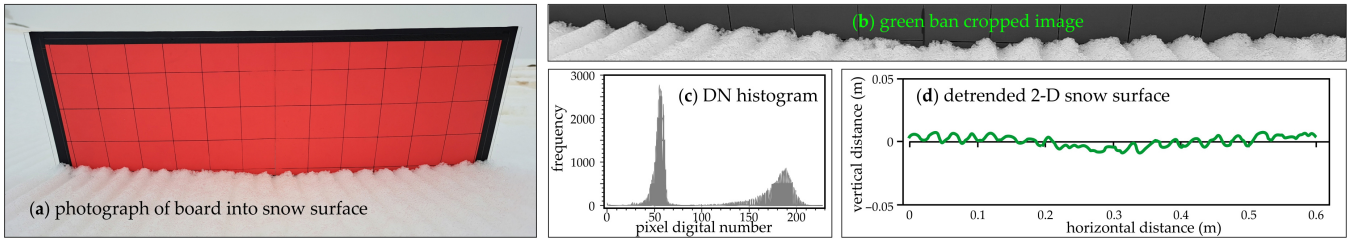

Figure 3. (**a**) Groomed snow board photo, (**b**) clipped green band image, (**c**) digital number (DN) distribution (board DN < 100), and (**d**) detrended snow surface. The board is 60 cm wide between the inside of the black edges.

3.1.1. Roughness Boards

A roughness board was used to define the directional snow surface roughness. The term directional is applied since the directional snow surface roughness is for a north–south or west–east line along the snow [5]. It represents one- and two-dimensional data [17].

A 60-cm wide snowboard was inserted into the snow so that the surface was fully contrasted by the board (Figure 3a). A photograph of the board was taken using a Samsung Galaxy A53 (SM-A536U1, 16 MP 4624 × 3468 pixels, ISO50, 24 mm) [39]. Each image was clipped horizontally to the black-red edge of the board (Figure 3b). The green band was converted to a matrix of digital numbers (DNs). Fassnacht et al. [17] showed that for a blackboard, the DN threshold was crucial; they used 140. Here, there were almost no pixels between 80 and 120 in the green band (Figure 3c). Thus, a DN threshold of 100 was used to identify the snow surface, i.e., board (low DN) versus snow (high DN) (Figure 3c).

Once the directional snow surface was converted into ASCII data, it was detrended to remove any slope bias from the angle of the surface and/or camera (Figure 3d). The full method is detailed in Fassnacht et al. [17]. The raw images are in JPEG format [40].

The roughness boards were inserted parallel (Figure 3a) and perpendicular to the grooming tracks (Table 1). The surface of the roughness board perpendicular to the grooming tracks is shown between the groomed tracks. Some areas of natural snow had some small undulations, while others showed sun cups (Figure 1).

3.1.2. iPad Surface Scans

The full snow surface was scanned to represent between 2- and 3-dimensions [23]. Surface scanning with an iPad has been shown to produce similar results to Terrrestrial Lidar scanning [41,42], ranging from a 4 mm error for features smaller than 5 cm [42] to 18 mm for larger elements [41]. Thus, the surfaces were scanned at a distance of about 1 m from the surface with an iPad Pro (4th generation) [43] using the 3-D Scanner App version 2.4.3 [44] (Figure 4). The software identifies a triangular mesh over the surface, and the iPad was moved over all triangles in the mesh until the desired area was scanned (Figure 4). While the specific scanning mechanism is proprietary and likely software-dependent, it appears to be structure-from-motion with lidar from a distance.

An 0.8 m × 1.6 m rectangular area was clipped in CloudCompare [45] for the dust-covered natural, sun-cupped natural (left in Figure 4), within the groomer tracks, and between the groomer tracks (right in Figure 4). Each area was examined to visually assess

for outliers, which were removed. Each area was detrended in X and Y [17], and the point cloud was interpolated to a 1-cm resolution using kriging and a Gaussian model with the Golden SURFER program [46]. Since the point cloud was at about a 1-cm resolution, the point cloud and the interpolation surface are at the same resolution, and many interpolation procedures could be used. The procedure is detailed in Neville et al. [7]. The raw, unclipped scan is an ASCII file with coordinates (X, Y, Z) and colour (R, G, B) [40].

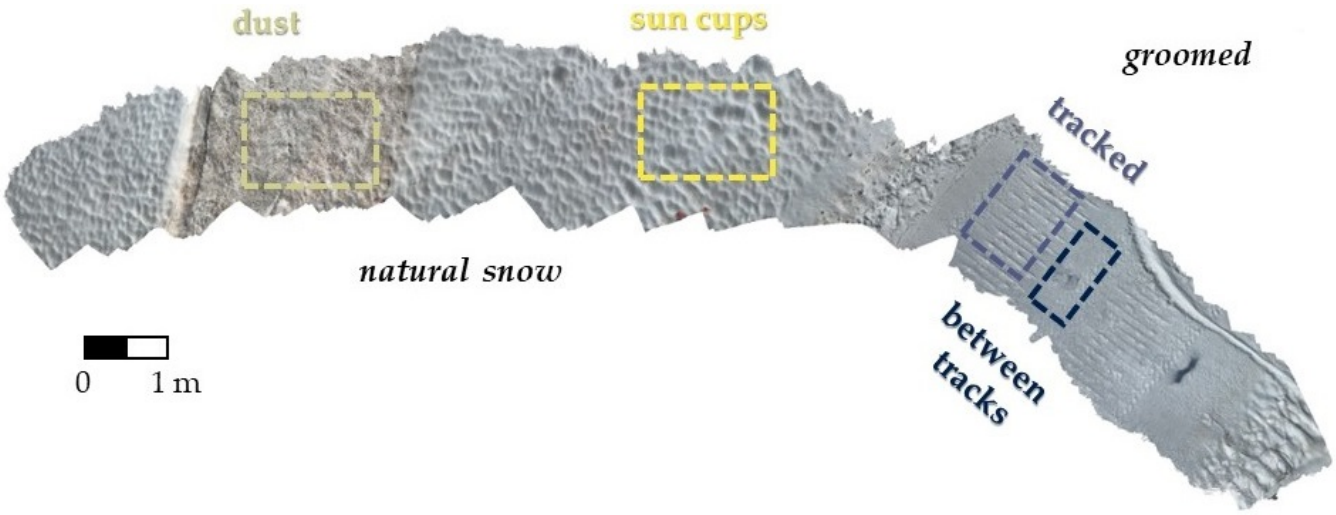

Figure 4. iPad snow surface scan RGB photograph illustrating natural snow (**left**) with dust on the surface and sun cups, and machine-groomed areas (**right**) as tracked and between tracks.

3.2. Roughness Evaluation

We used a variety of metrics to assess snow surface roughness [17]. The Random Roughness (RR) is the standard deviation of the detrended surface. It does not consider the spatial structure or relative location of any surface point.

Variogram analysis considers the spatial structure of the surface. It was used to compute the Scale Break (SB) and Fractal Dimension (D). Variograms were computed for each surface, with lag distance being in logarithmic bins and semi-variance also being in logarithmic space [47]. In log-log space, any change in a linear segment represented a potential SB. A power function (line in log-log space) was fit to the points, and the best-fit was optimized using the correlation coefficient by adjusting the range of the lag distance. The value of D was computed as 2 or 3 minus the exponent in the power function divided by 2 [47] for the roughness boards or iPad scans, respectively.

The geometric-based aerodynamic roughness length (z_0) was derived from the full snow surface (iPad scans). The geometric z_0 value was computed using the Lettau [48] method with the watershed-identification code of Neville et al. [7]. The Lettau [48] equation is presented in Appendix A (Equation (A1)).

3.3. Sublimation Estimation

One-minute meteorological data were collected for four hours (10:19 to 14:32) at the field site [49]. A Vaisala WXT510 Weather Transmitter (Vaisala Oyj, Vanha Nurmijärventie 21, Vantaa, Finland) [50] was used to measure wind speed (at a height of 0.7 m above the snowpack), temperature, and relative humidity (0.6 m above the snowpack). Snow surface temperature was collected using a Campbell Scientific 109 Temperature Probe (Campbell Scientific, Logan, UT, USA) [51]. Both sensors were connected to a Campbell Scientific CR200 datalogger (Campbell Scientific, Logan, UT, USA) [52].

The meteorological data were used with the calculated geometric-based z_0 values to compute the bulk-transfer sublimation (Appendix A; Equation (A2)) [53]. Concurrently,

evapo-sublimation pans [54] were deployed in the groomed and ungroomed areas to provide field measurements of sublimation-evaporation and melt [35]. These field data are not presented in this analysis, as the focus is on the variability of roughness at a ski area and the potential impact of snow surface geometry on sublimation modelling.

4. Results

The groomed snow was much smoother than the ungroomed snow, especially when sun cups were present (Figures 4 and 5). Grooming provided relatively homogeneous grooves (Figure 5a) and the area between the tracks was essentially flat (Figure 5b). The natural surface had some undulations (Figure 5c) that were enhanced where sun cups formed (Figure 5d).

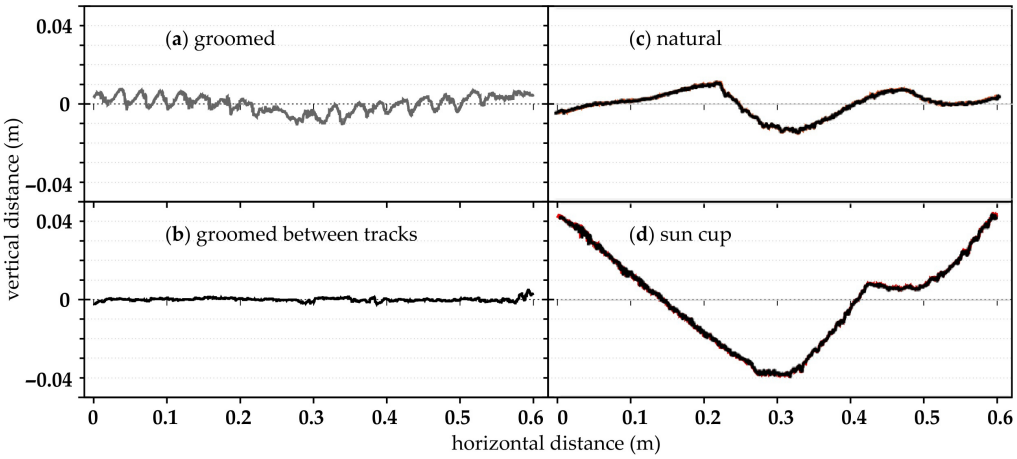

Figure 5. Snow board geometry for the groomed surface (**a**) parallel versus (**b**) perpendicular to grooming), (**c**) natural snow, and (**d**) in the presence of sun cups.

The four surfaces interpolated from the iPad scans (Figure A1) exhibited distinct spatial variability. Despite these visual differences, the roughness of the iPad-scanned surfaces (Figure A1) broadly matched that from the roughness boards (Figure 5). Variograms illustrated the same roughness structure between the same features (Figure 6), although the order of magnitude of the roughness differed between methods (Figure A2).

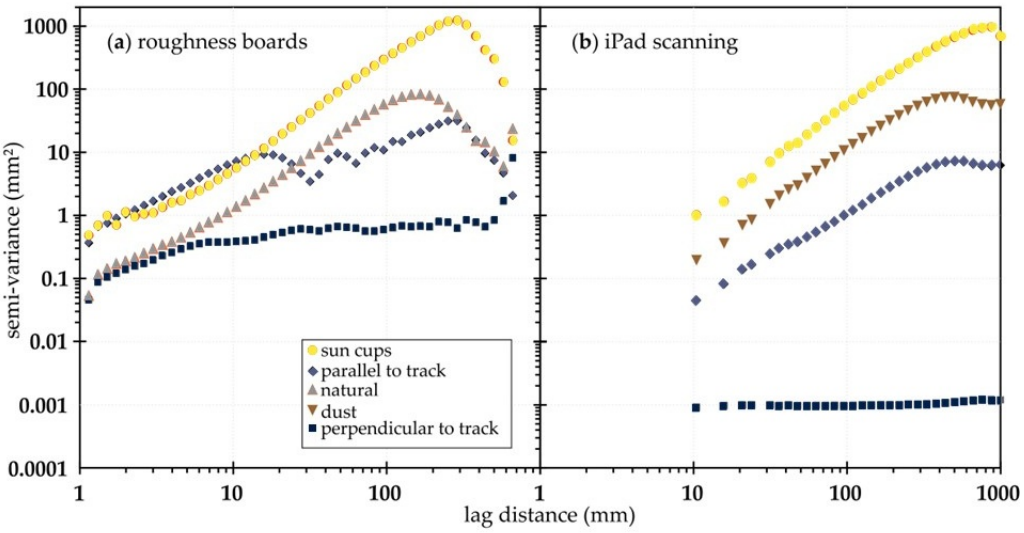

Figure 6. Variograms for the (**a**) roughness boards (2-D data) and the (**b**) iPad scans (3-D data).

The scale breaks (SBs), or change in slope in the variograms (Figure 6), were in a similar range for the two measurement types (boards versus scans), though they did not match exactly. The fractal dimensions (D) were more similar among the surfaces (Figure 7). Similarly, RR values were almost the same between the roughness boards (Figure 7a) and the iPad scans (Figure 7b).

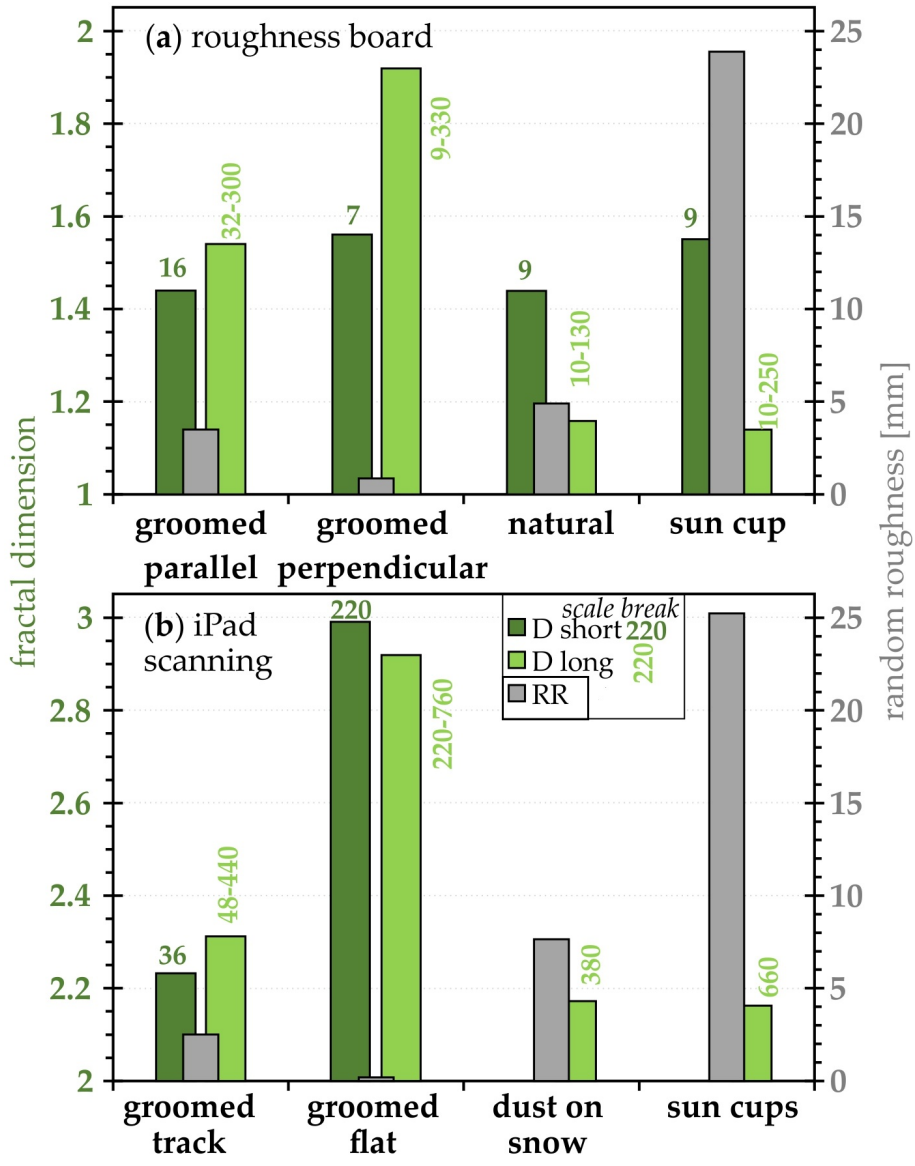

Figure 7. Fractal Dimension (D) values on the left with bars in dark (light) green for short (long) lag distance derived from variogram analysis (Figure 6), plus the Random Roughness (RR) values on the right in grey. The horizontal number is the Scale Break (SB) in mm for the short lag, and the vertical numbers are the range of scales for the long lag. Plots are for (**a**) roughness boards and (**b**) iPad scanning.

RR values are largest for the sun cups, and thus most organized, i.e., D was smallest for the longer scales (light green in Figure 7) where D = 1.15 for the roughness board and D = 2.15 for the iPad surface. For the shorter scales (dark green), D was similar to the grooming surface (up to 16 mm, which was the period of the groomer teeth; Figures 3 and 5a), and for the natural and sun cups board and iPad surface. For the latter two, D of about 1.5, for a distance of 7 mm, represented the rounded snow grains. The board parallel to grooming was almost flat, and the surface was more random (D was larger).

The default z_0 modelling value was 0.24 mm. The geometric-based z_0 for the groomed surface was almost the same (0.35 mm) (Figure 8). The other z_0 values matched the pattern in RR, with low RR values (groomed flat) yielding low z_0 values and larger roughness surfaces, i.e., sun cups, being larger (z_0 of 9.5 mm). The variations in z_0 influenced the modelled sublimation estimates (Figure 9), illustrating an order of magnitude of variation.

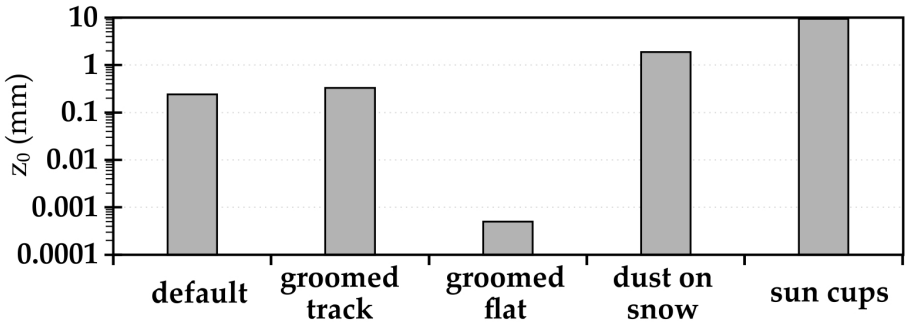

Figure 8. Geometric-based z_0 estimates using the approach of Neville et al. [7].

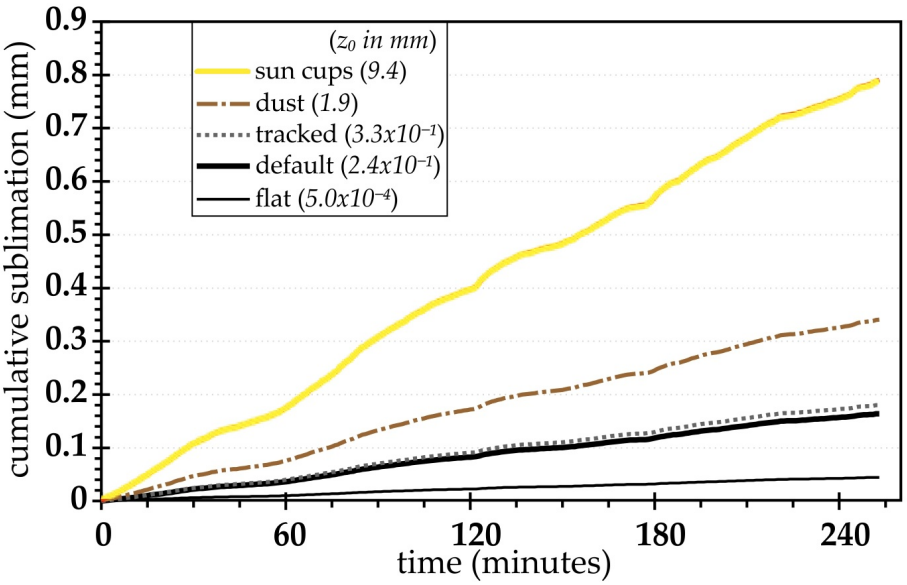

Figure 9. Modelled cumulative snowpack sublimation from the bulk transfer approach using the z_0 estimates from Figure 8.

5. Discussion

5.1. Roughness Assessment

There is consistency in the roughness features across scales, i.e., between the roughness boards and the iPad scanning (Figures 6 and 7). Sun cups had the largest roughness (largest magnitude in the variograms and largest RR) and were most organized (lowest D), while the groomed surface between the tracks was smoothest and most random [17]. The tracked surfaces were similar (Figures 7 and A2). While we did not measure the dust on the snow surface with the roughness boards, its roughness was also similar to the natural snow without the sun cups (Figure 6). We measured the natural snow (without sun cups) at two locations in both the north-south and west-east directions. These four variograms were essentially on top of one another, illustrating consistency among the same surface form.

The roughness features presented herein (Figures 1 and 4) were seen across the ski area during travel to and from the study site (Figure 2). While it is not practical to map these features across an entire ski area, their smaller-scale structure was evaluated (Figures 6 and 7). Unmanned Aerial Vehicles (UAVs) could be used to assess the location of different fea-

tures [55]. While it is currently not known if the small-scale features can be measured with a UAV, it is possible that combining the data with the spectral signature could differentiate the features (e.g., colours in Figure 4).

This current work can be expanded upon to provide a comparison of different metrics for assessing snow surface roughness [17], especially across scales [23]. Lettau [48] used geometry to estimate z_0 from roughness elements, here defined as watersheds [7] (Figure A1); other approaches used a transect of roughness [56]. Such approaches could be combined to use variables such as RR and D to estimate z_0. Further, the roughness features presented herein (Figures 1, 4, 5 and A1) are a portion of the general snow roughness classification by the International Association of Cryospheric Sciences [57]. This could be expanded to include machine-made (Figure 5a,b) and other roughness elements.

5.2. Sublimation

A ski area can have a variety of snow surfaces (Figures 5 and A1) with different roughness (Figures 6 and 7) that will impact wind movement across the surface. Using a geometric approach [48], this yields varying z_0 values (Figure 8) that produce a variety of sublimation estimates (Figure 9). Sublimation is an important process in the water balance of mountainous regions [58]. Sublimation and melt-evaporation [35] on ski slopes will influence snow making due to consumptive use [59–61]. These processes need to be implemented into models [62], especially due to reduced reliability of snow under climate change [63].

The aerodynamics will vary due to geometry (Figure 8). However, these aerodynamic differences will be less when compared to the surface variation of the snowpack. To better quantify sublimation losses and to evaluate the sensitivity of the roughness controls, concurrent measurements from sublimation pans would be useful [35,54]. Further, while the geometric-based z_0 values are comparable to those derived from anemometers [64], it is useful to estimate measure z_0 from anemometers [65] and geometry [48].

5.3. Surface Measurement

The iPad scanning appears unable to resolve the flat snow surface (Figure 6b), especially compared to the roughness board (Figure A2). The iPad flat surface between the tracks (Figure A1b) was essentially random (D = 2.99; Figures 6b and 7b). Conversely, the surface is completely flat, and thus D would be 2, i.e, a plane. The iPad cannot resolve such a difference. Further, artifacts arise from iPad data collection and the nature of photogrammetry processing. Roughness metrics on flat surfaces may be biased. UAVs are now used to measure the snowpack [55], but these also cannot resolve such differences.

For the roughness board, there was some order (D = 1.56) at the shorter scale (up to 7 mm) (Figures 5b and 7a), but this was not picked up by the iPad scanning. The iPad scanning with the software used herein (3D Scanner App) has been shown to resolve features smaller than 5 cm with a 4 mm error in the best case [42], but 1–2 cm off in other studies [41,66]. For the longer scale, there was the same slight order (D = 1.92 and 2.92 for the board and iPad, respectively). The interpolated iPad surface appears to have much roughness (polygons in Figure A1a), but these are all plus or minus zero and less than 5 mm.

The actual process for creating the point cloud from iPad scanning [43,44] is proprietary, and more information is needed to determine the accuracy of scanning smooth snow surfaces. It is recommended that this scanning be compared with data collected from terrestrial lidar (e.g., [3]), specifically for snow, due to its high reflectance. Here, we used the 3D Scanner App [44]; other software could also be evaluated [41]. However, for the

rougher surfaces (natural, dust, and sun cups), the iPad surfaces (1 cm resolution) seemed to match the roughness boards (0.2 mm resolution).

The iPad scanning also produces a point cloud of RGB colour returns (Figure 4). These data could be used to estimate albedo in the visible portion of the spectrum [67]. At our study area, this is relevant due to the presence of dust (Figure 1), which lowers albedo, increases snow melt [68], and changes snow roughness [5].

5.4. Limitations

The scope of this work is limited to investigating the nature of the snow surfaces that can be observed at one ski resort during melt, specifically focusing on several roughness metrics. This paper did not examine sublimation across the entire ski resort. However, investigating the degree of difference in snow surface roughness illustrates its importance for the energy balance, specifically sublimation. Meteorological data [49] were collected on the edge between the groomed and ungroomed (natural) surfaces. Future work should collect such data over each of the various surfaces (Figure 4). The iPad surface-scanning for snowpacks has not been evaluated and should be compared with terrestrial lidar scanning. The resolution versus extent (low on iPad) should also be examined; UAVs are the preferred data-collection method for snow depth [55], but it is unclear if such hardware collects data at the necessary resolution to resolve features like grooming (Figure 3). The geometry of the snowpack surface is a surrogate for z_0 [7,48], but it may not represent the anemometric-based z_0 [12,64]. Erroneous measurements from the iPad or other surfaces used for mapping could propagate errors into sublimation modelling. However, these are lower than with a default, constant z_0 value. The roughness of the snowpack varies, and this impacts the energy balance in various ways.

6. Conclusions

In this paper, we examined the various snowpack surfaces with different roughness levels that are found at ski areas during snowmelt. We then used those different roughnesses in a sensitivity analysis of sublimation modelling. The snowpack at a ski resort can vary in surface conditions. At the Sierra Nevada ski area, investigated here, we observed two natural surfaces with the presence of dust and sun cups and two groomed surfaces with rills from the tracks and a flatter surface between. The sun cup surface had the most roughness, followed by the natural and dust-covered surfaces. Both showed similar roughness values with the finer-resolution 2-D roughness board and the coarser-resolution 3-D iPad scanning. The tracked 3-D surface was similar to the board, while the flat surface was less similar among the methods. This was likely due to the iPad scanning not resolving features on the flat surface.

There is a large difference between how much sublimation we model for different parts of a ski resort. The aerodynamics of near-surface meteorology are influenced by various snow surface roughnesses, which, in turn, alter snow surface characteristics. We computed the geometric-based z_0 from the surface geometry. Future work should examine the anemometric-based z_0, and also use snow/earth system models that better estimate all components of the energy balance.

The results from this work are robust. The differences between the various snow surfaces are large, as indicated by the metrics and sublimation modelling. While simple techniques were used to measure the various surfaces, there is consistency between methods (roughness boards and iPad).

The use of a constant z_0 value for all snowpack surfaces is wrong. The snowpack surface is dynamic and varies over space (here) and time. This needs to be considered for

the snowpack energy balance and beyond. The sublimation sensitivity analysis illustrates the importance of accounting for variable and dynamic snow surface roughness.

The implications of this work are for the computation of consumptive loss of snow at a ski area. This includes natural and machine-made snow. This could help identify areas where more snowmaking should occur and/or for ski slope maintenance from surrounding areas with less sublimation. While this study focused on a single small area at a single ski resort, the different surfaces examined herein were observed across the resort. Remote sensing, such as high-resolution satellite imagery and UAVs (Unmanned Aerial Vehicles), can be used to map the different snow roughness features or an entire ski area.

Author Contributions: Conceptualization, S.R.F. and J.H.; methodology, S.R.F., J.H. and J.E.S.; software, S.R.F.; validation, S.R.F., J.H. and J.E.S.; formal analysis, S.R.F., J.H. and J.E.S.; investigation, S.R.F. and J.H.; resources, S.R.F. and J.H.; data curation, S.R.F. and J.H.; writing—original draft preparation, S.R.F.; writing—review and editing, S.R.F., J.H., and J.E.S.; visualization, S.R.F.; project administration, J.H. and S.R.F.; funding acquisition, S.R.F. and J.H. All authors have read and agreed to the published version of the manuscript.

Funding: This research was funded by the QUALIFICA Project (Modeling Nature/QUAL21-11), funded by Granada-CETURSA Sierra Nevada S.A. (UGR OTRI-6429), funded by the Regional Ministry of University, Research and Innovation of the Junta de Andalucía. SRF was supported by the Fulbright Global Scholar program during this research.

Institutional Review Board Statement: Not applicable.

Informed Consent Statement: Not applicable.

Data Availability Statement: The original data presented in the study are openly available at [40]. The meteorological data are in the process of being published [49].

Acknowledgments: We thank the Sierra Nevada Ski Area for their support. We thank the four anonymous reviewers for their excellent comments, which helped improve the scope of this paper. Reviewer 2 was particularly helpful with the suggestion to adopt perceptually uniform, colour-blind-safe palettes. We used Cividis. Thank you "blind" reviewer.

Conflicts of Interest: The authors declare no conflicts of interest. The funders had no role in the design of the study; in the collection, analyses, or interpretation of data; in the writing of the manuscript; or in the decision to publish the results.

Appendix A. Equations Used

The Lettau [48] equation for individual roughness elements is utilized:

$$z_0 = 0.5h\frac{s}{S}, \tag{A1}$$

where h is the "average vertical extent," or "effective obstacle height," measured in cm, s is the "silhouette area of the average obstacle," measured in cm^2, and S is the "specific area", or "lot area", measured in cm^2 [48].

The bulk transfer equation [53] was used to estimate the mass of sublimation (E):

$$E = -0.622\frac{\rho_a}{Pr_a}k^2\frac{U_z}{LN(z_U/z_0)}\frac{(e_a - e_0)}{LN(z_T/z_0)}, \tag{A2}$$

where ρ_a is the density of air (kg/m^3), Pr_a is the air pressure (mb), k 0.4 (von Karman coefficient), U_z is the wind speed (m/s), z_U is the wind speed measurement height (m), e_a is the vapour pressure at the sensor height (mb) computed from air temperature and humidity, e_0 is the surface vapour pressure (mb), and z_T is the temperature and humidity measurement height (m). The values of z_0 are computed from [7].

Appendix B. Interpolated iPad Scan Surfaces

The appendix presents the clipped iPad scanned surfaces (Figure 4), which were interpolated to an area of 0.8 × 1.6 m (Figure A1).

The iPad-derived tracked surface (Figure A1a) did not show the consistent rills as the roughness board interface (Figures 3 and 5a).

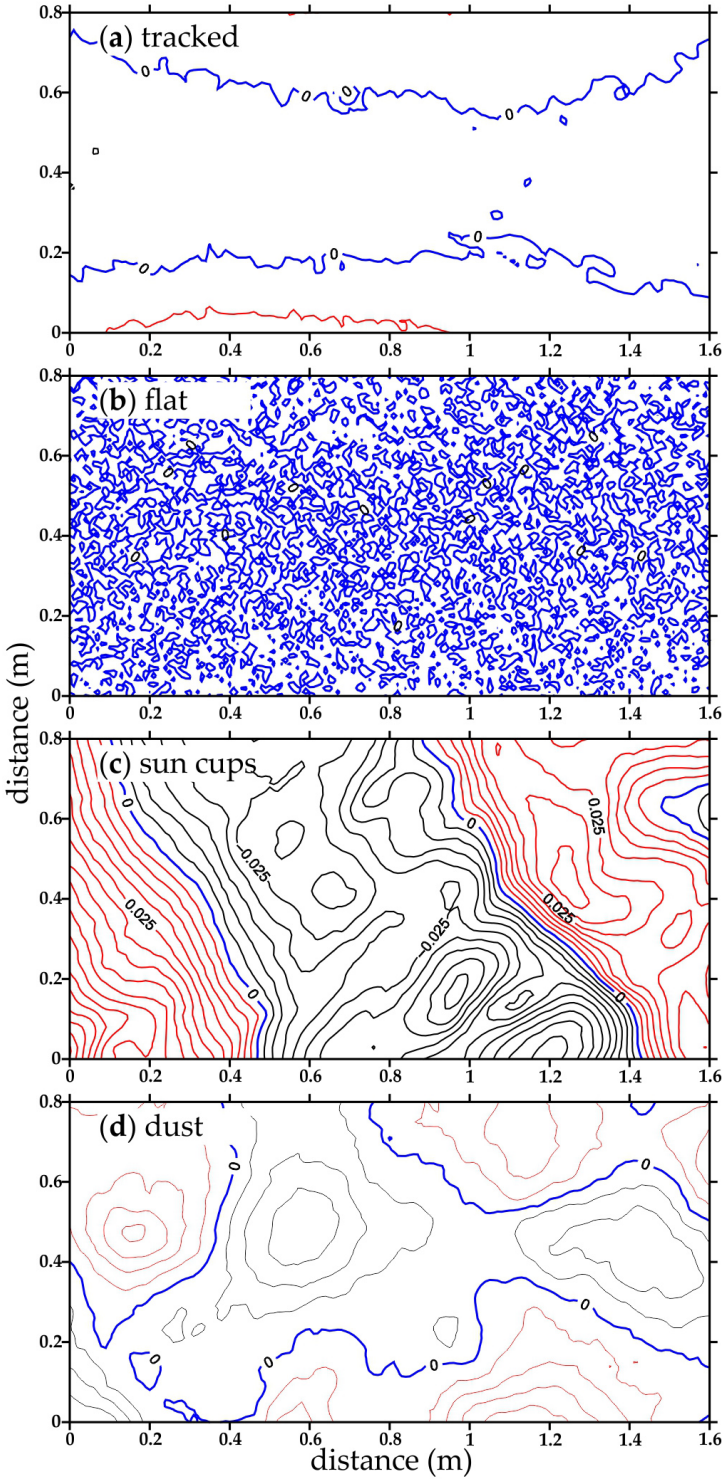

Figure A1. The four 1 cm resolution interpolated snow surfaces from the iPad scanning illustrated with contour intervals of 0.005 m (5 mm) and labelled at 0.025 m intervals for (**a**) tracked surface, (**b**) flat surface between tracks, (**c**) sun cups, and (**d**) dust on snow. The data were detrended prior to interpolating. The zero line is presented in blue, with negative contours in black and positive in red.

Appendix C. Variograms over Scales and Dimensions

This Appendix presents a comparison of the semi-variance for the four overlapping iPad scanning surfaces versus the roughness boards curves (Figure A2).

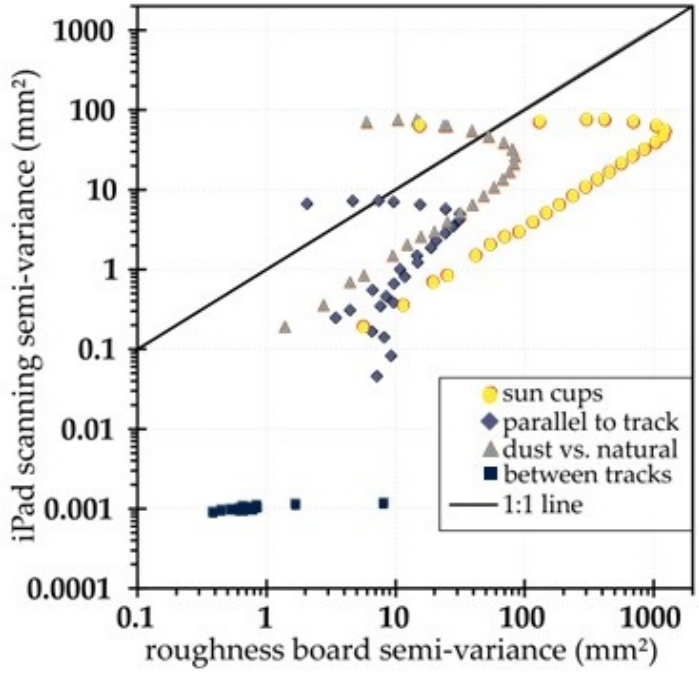

Figure A2. Comparison of the semi-variance for the iPad scanning surfaces versus the roughness board curves.

References

1. Kohnen, G. (Black Forest Gardens, King City, Ontario, Canada). Personal Communication, 1995.
2. Veitinger, J.; Sovilla, B.; and Purves, R.S. Influence of snow depth distribution on surface roughness in alpine terrain: A multi-scale approach. *Cryosphere* **2014**, *8*, 547–569. [CrossRef]
3. Sanow, J.E.; Fassnacht, S.R. Let Us Change the Aerodynamic Roughness Length as a Function of Snow Depth. *Climate* **2025**, *13*, 226. [CrossRef]
4. Brock, B.; Willis, I.; Sharp, M. Measurement and parameterization of aerodynamic roughness length variations at Haut Glacier d'Arolla, Switzerland. *J. Glaciol.* **2006**, *52*, 281–297. [CrossRef]
5. Fassnacht, S.R.; Williams, M.; Corrao, M. Changes in the surface roughness of snow from millimetre to metre scales. *Ecol. Complex.* **2009**, *6*, 221–229. [CrossRef]
6. Van Tiggelen, M.; Smeets, P.C.; Reijmer, C.H.; Van den Broeke, M.R. A vertical propeller eddy-covariance method and its application to long-term monitoring of surface turbulent fluxes on the Greenland ice sheet. *Bound.-Layer Meteorol.* **2020**, *176*, 441–463. [CrossRef]
7. Neville, R.A.; Shipman, P.D.; Fassnacht, S.R.; Sanow, J.E.; Pasquini, R.; Oprea, I. A New Formulation and Code to Compute Aerodynamic Roughness Length for Gridded Geometry—Tested on Lidar-derived Snow Surfaces. *Remote Sens.* **2025**, *17*, 1984. [CrossRef]
8. Mitchell, K.A.; Tiedje, T. Growth and fluctuations of suncups on alpine snowpacks. *J. Geophys. Res.* **2010**, *115*, F04039. [CrossRef]
9. Fassnacht, S.R.; Toro Velasco, M.; Meiman, P.J.; Whitt, Z.C. A Local Aeolian Influence in the Surface Roughness of Melting Snow, Byers Peninsula, Antarctica. *Hydrol. Process.* **2010**, *24*, 2007–2013. [CrossRef]
10. Sverdrup, H.U. Scientific Results of the Norwegian-Swedish Spitsbergen Expedition in 1934. Part VI-VII. *Geogr. Ann.* **1936**, *18*, 34–73. [CrossRef]
11. Oke, T.R. *Boundary Layer Climates*, 2nd ed.; Routledge: Oxfordshire, UK , 1987; 464p.
12. Andreas, E.L. A theory for the scalar roughness and the scalar transfer coefficients over snow and sea ice. *Bound.-Layer Meteorol.* **1987**, *38*, 159–184. [CrossRef]
13. Anderson, E.A. Development and testing of snow pack energy balance equations. *Water Resour. Res.* **1968**, *4*, 19–37. [CrossRef]
14. Marks, D.; Dozier, J. Climate and energy exchange at the snow surface in the alpine region of the Sierra Nevada: 2. Snow cover energy balance. *Water Resour. Res.* **1992**, *28*, 3043–3054. [CrossRef]

15. Van den Broeke, M.R.; Smeets, P.C.J.P.; van de Wal, R.S.W. The seasonal cycle and interannual variability of surface energy balance and melt in the ablation zone of the west Greenland ice sheet. *Cryosphere* **2011**, *5*, 377–390. [CrossRef]
16. Wang, W.; Zender, C.S.; As, D.V.; Fausto, R.S.; Laffin, M.K. Greenland surface melt dominated by solar and sensible heating. *Geophys. Res. Lett.* **2021**, *48*, 1–16. [CrossRef]
17. Fassnacht, S.R.; Stednick, J.D.; Deems, J.S.; Corrao, M.V. Metrics for assessing snow surface roughness from digital imagery. *Water Resour. Res.* **2009**, *45*, W00D31. [CrossRef]
18. UCAR. Community Land Model (CLM). Available online: https://www.cesm.ucar.edu/models/clm (accessed on 21 October 2025).
19. Manninen, T.; Anttila, K.; Jääskeläinen, E.; Aku Riihelä, A.; Peltoniemi, J.; Räisänen, P.; Lahtinen, P.; Siljamo, N.; Thölix, L.; Meinander, O.; et al. Effect of small-scale snow surface roughness on snow albedo and reflectance. *Cryosphere* **2021**, *15*, 793–820. [CrossRef]
20. Anttila, K.; Manninen, T.; Karjalainen, T.; Lahtinen, P.; Riihelä, A.; Siljamo, N. The temporal and spatial variability in submeter scale surface roughness of seasonal snow in Sodankylä Finnish Lapland in 2009–2010. *J. Geophys. Res.* **2014**, *119*, 9236–9252. [CrossRef]
21. Morin, S.; François, H.; Réveillet, M.; Sauquet, E.; Crochemore, L.; Branger, F.; Leblois, É.; Dumont, M. Simulated hydrological effects of grooming and snowmaking in a ski resort on the local water balance. *Hydrol. Earth Syst. Sci.* **2023**, *27*, 4257–4277. [CrossRef]
22. Hanzer, F.; Carmagnola, C.M.; Ebner, P.P.; Koch, F.; Monti, F.; Bavay, M.; Bernhardt, M.; Lafaysse, M.; Lehning, M.; Strasser, U.; et al. Simulation of snow management in Alpine ski resorts using three different snow models. *Cold Reg. Sci. Technol.* **2020**, *172*, 102995. [CrossRef]
23. Fassnacht, S.R.; Suzuki, K.; Sanow, J.E.; Sexstone, G.A.; Pfohl, A.K.D.; Tedesche, M.E.; Simms, B.M.; Thomas, E.S. Snow Surface Roughness across Spatio-Temporal Scales. *Water* **2023**, *15*, 2196. [CrossRef]
24. Camarero, J.J.; Gazol, A.; Tamudo, E.; Moiseev, P.A.; Colangelo, M.; Valeriano, C. Local and regional climatic constraints of shrub and tree growth near the treeline. *Dendrochronologia* **2024**, *88*, 126256. [CrossRef]
25. Flynn, H.; Camarero, J.J.; Sanmiguel-Vallelado, A.; Rojas Heredia, F.; Domínguez Aguilar, P.; Revuelto, J.; López-Moreno, J.I. A shift in circadian stem increment patterns in a Pyrenean alpine treeline precedes spring growth after snow melting. *Biogeosciences* **2025**, *22*, 1135–1147. [CrossRef]
26. Grabherr, G.; Nagy, L.; Thompson, D.B.A. An outline of Europe's alpine areas. In *Alpine Biodiversity in Europe*; Springer: Berlin/Heidelberg, Germany, 2003; pp. 3–12.
27. Polo, M.J.; Herrero, J.; Millares, A.; Pimentel, R.; Moñino, A.; Pérez-Palazón, M.J.; Aguilar, C.; Losada, M.A. Snow Dynamics, Hydrology, and Erosion. In *The Landscape of the Sierra Nevada*; Zamora, R., Oliva, M., Eds.; Springer: Cham, Switzerland, 2022.
28. Gómez-Ortiz, A.; Oliva, M.; Salvà-Catarineu, M.; Salvador-Franch, F. The environmental protection of landscapes in the high semiarid Mediterranean mountain of Sierra Nevada National Park (Spain): Historical evolution and future perspectives. *Appl. Geogr.* **2013**, *42*, 227–239. [CrossRef]
29. Campos Rodrigues, L.; Freire-González, J.; González Puig, A.; Puig-Ventosa, I. Climate Change Adaptation of Alpine Ski Tourism in Spain. *Climate* **2018**, *6*, 29. [CrossRef]
30. Pardo-Igúzquiza, E.; Martos-Rosillo, S.; Jódar, J.; Dowd, P.A. The Spatio-Temporal Dynamics of Water Resources (Rainfall and Snow) in the Sierra Nevada Mountain Range (Southern Spain). *Resources* **2024**, *13*, 42. [CrossRef]
31. Molero, J.; Pérez-Raya, F. La Flora de Sierra Nevada. In *Avance Sobre el Catálogo Florístico Nevadense*; Universidad de Granada: Granada, Spain, 1987.
32. Lorite, J.; Molina-Morales, M.; Cañadas, E.M., Ballesteros, M.; Peñas, J. Evaluating a vegetation-recovery plan in Mediterranean alpine ski slopes: A chronosequence-based study in Sierra Nevada (SE Spain). *Landsc. Urban Plan.* **2010**, *97*, 92–97. [CrossRef]
33. Blanca, G.; López Onieva, M.R.; Lorite, J.; Martínez Lirola, M.J.; Molero, J.; Quintas, S.; Ruiz Girela, M.; de los Ángeles Varo Santiago Vidal, M. *Flora Amenazada y endéMica de Sierra Nevada*; Universidad de Granada: Granada, Spain; Consejería de Medio Ambiente, Junta de Andalucía: Sevilla, Spain, 2001; ISBN 84-338-2713-8.
34. Collados-Lara, A.; Pardo-Igúzquiza, E.; Pulido-Velazquez, D.; Jiménez-Sánchez, J. Precipitation fields in an alpine Mediterranean catchment: Inversion of precipitation gradient with elevation or undercatch of snowfall? *Int. J. Climatol.* **2018**, *38*, 3565–3578. [CrossRef]
35. Herrero, J.; Polo, M.J. Evaposublimation from the snow in the Mediterranean mountains of Sierra Nevada (Spain). *Cryosphere* **2016**, *10*, 2981–2998. [CrossRef]
36. Collados-Lara, A.J.; Pardo-Igúzquiza, E.; Pulido-Velazquez, D. Assessing the impact of climate change–and its uncertainty–on snow cover areas by using cellular automata models and stochastic weather generators. *Sci. Total Environ.* **2021**, *788*, 147776. [CrossRef] [PubMed]
37. Rixen, C.; Haeberli, W.; Stoeckli, V. Ground temperatures under ski pistes with artificial and natural snow. *Arctic, Antarct. Alp. Res.* **2004**, *36*, 419–427. [CrossRef]

38. Yoshizawa, N.; Cognard, J.; Berard-Chenu, L.; Bourdeau, P. Off-Piste Skiing Demand Patterns and Climate Change Adaptation Pathways in La Grave, France. *Mt. Res. Dev.* **2025**, *45*, R9–R18. [CrossRef]
39. Samsung. Galaxy A53. Available online: https://www.samsung.com/latin_en/smartphones/galaxy-a/galaxy-a53-5g-awesome-black-128gb-sm-a536ezkdtpa/ (accessed on 10 November 2025).
40. Fassnacht, S.R.; Herrero, J. Sierra Nevada Spain Snow Surface Data at the Ski Area 2024. *Pangaea* **2026** . https://doi.pangaea.de/10.1594/PANGAEA.989349. [CrossRef]
41. Nelson, P. Evaluation of Handheld Apple iPad Lidar for Measurements of Topography and Geomorphic Change. *Authorea* **2021** . [CrossRef]
42. Monsalve, A.; Yager, E.M.; Tonina, D. Evaluating Apple iPhone LiDAR measurements of topography and roughness elements in coarse bedded streams. *J. Ecohydraulics* **2025**, *10*, 181–191. [CrossRef]
43. Apple. iPad Pro. Available online: https://www.apple.com/ipad-pro/ (accessed on 10 November 2025).
44. labs.claan.com. 3D Scanner App. Available online: https://3dscannerapp.com/ (accessed on 10 November 2025).
45. Available online: https://www.danielgm.net/cc/ (accessed on 7 June 2025).
46. Golden Software. Available online: https://www.goldensoftware.com/products/surfer/ (accessed on 11 November 2025).
47. Deems, J.S.; Fassnacht, S.R.; Elder, K.J. Fractal distribution of snow depth from LiDAR data. *J. Hydrometeorol.* **2006**, *7*, 285–297. [CrossRef]
48. Lettau, H. Note on Aerodynamic Roughness-Parameter Estimation on the Basis of Roughness-Element Description. *J. Appl. Meteorol.* **1969**, *8*, 828–832. [CrossRef]
49. Herrero, J. Meteorological and Snow Data Collected during Sublimation and Melt Experiments at the Sierra Nevada Ski Resort (Spain), Spring 2024 [Data set]. Zenodo 2026, 18294384. Available online: https://zenodo.org/records/18294384 (accessed on 11 November 2025).
50. Vaisala. WXT510 User Guide in English. 2006 . Available online: https://www.vaisala.com/sites/default/files/documents/WXT510_User_Guide_in_English.pdf-mutedduetoerrorfromtheunderscores (accessed on 18 January 2026).
51. Campbell Scientific. 109 Temperature Probe. 2026 . Available online: https://www.campbellsci.com/109 (accessed on 18 January 2026).
52. Campbell Scientific. CR200 Data Logger. 2026 . Available online: https://www.campbellsci.com/cr200 (accessed on 18 January 2026).
53. Reba, M.L.; Pomeroy, J.; Marks, D.; Link, T.E. Estimating surface sublimation losses from snowpacks in a mountain catchment using eddy covariance and turbulent transfer calculations. *Hydrol. Process.* **2012**, *26*, 3699–3711. [CrossRef]
54. Beaty, C.B. Sublimation or melting: Observations from the White Mountains, California and Nevada, USA. *J. Glaciol.* **1975**, *14*, 275–286. [CrossRef]
55. Revuelto, J.; Alonso-Gonzalez, E.; Vidaller-Gayan, I.; Lacroix, E.; Izagirre, E.; Rodríguez-López, G.; López-Moreno, J.I. Intercomparison of UAV platforms for mapping snow depth distribution in complex alpine terrain. *Cold Reg. Sci. Technol.* **2021**, *190*, 103344. [CrossRef]
56. Andreas, E.L. A relationship between the aerodynamic and physical roughness of winter sea ice. *Q. J. R. Meteorol. Soc.* **2011**, *137*, 1581–1588. [CrossRef]
57. Fierz, C.R.L.A.; Armstrong, R.L.; Durand, Y.; Etchevers, P.; Greene, E.; et al. The International Classification for Seasonal Snow on the Ground. International Association of Cryospheric Sciences 2009, IHP Technical Documents in Hydrology No. 83, IACS Contribution No. 1. Available online: https://cryosphericsciences.org/publications/snow-classification/ (accessed on 2 March 2026).
58. Strasser, U.; Bernhardt, M.; Weber, M.; Liston, G.E.; Mauser, W. Is snow sublimation important in the alpine water balance? *Cryosphere* **2008**, *2*, 53–66. [CrossRef]
59. Smart, A.W.; Fleming, W.M. *Consumptive Water Use in Artificial Snowmaking Santa Fe Ski Area. New Mexico (No. 45–46)*; New Mexico State Engineer Office: Albuquerque, NM, USA, 1985.
60. Eisel, L.M.; Mills, K.D.; Leaf, C.F. Estimated Consumptive Loss from Man-made Snow. *J. Am. Water Resour. Assoc.* **1988**, *24*, 815–820. [CrossRef]
61. Eisel, L.M.; Bradley, K.M.; Leaf, C.F. Estimated Runoff from Man-made Snow. *J. Am. Water Resour. Assoc.* **1990**, *26*, 519–526. [CrossRef]
62. Krinner, G.; Derksen, C.; Essery, R.; Flanner, M.; Hagemann, S.; Clark, M.; Hall, A.; Rott, H.; Brutel-Vuilmet, C.; Kim, H.; et al. ESM-SnowMIP: Assessing snow models and quantifying snow-related climate feedbacks. *Geosci. Model Dev.* **2018**, *11*, 5027–5049. [CrossRef]
63. Spandre, P.; François, H.; Verfaillie, D.; Pons, M.; Vernay, M.; Lafaysse, M.; George, E.; Morin, S. Winter tourism under climate change in the Pyrenees and the French Alps: Relevance of snowmaking as a technical adaptation. *Cryosphere* **2019**, *13*, 1325–1347. [CrossRef]

64. Sanow, J.E.; Fassnacht, S.R.; Kamin, D.J.; Sexstone, G.A.; Bauerle, W.L.; Oprea, I. Geometric Versus Anemometric Surface Roughness for a Shallow Accumulating Snowpack. *Geosciences* **2018**, *8*, 463. [CrossRef]
65. Andreas, E.L. Parameterizing scalar transfer over snow and ice: A review. *J. Hydrometeorol.* **2002**, *3*, 417–432. [CrossRef]
66. Abdel-Majeed, H.M.; Shaker, I.F.; Abdel-Wahab, A.M.; Awad, A.A.D.I. Indoor mapping accuracy comparison between the apple devices' LiDAR sensor and terrestrial laser Scanner. *HBRC J.* **2024**, *20*, 915–931. [CrossRef]
67. Gaillard, M.; Vionnet, V.; Lafaysse; M.; Dumont, M.; Ginous, P. Improving large-scale snow albedo modelling using a climatology of light-absorbing particle deposition. *Cryosphere* **2025**, *19*, 769–792. [CrossRef]
68. Miller, G.; Jennifer, D. Big Takeover. In *Tracks 11 on Bad Brains*; ROIR: New York, NY, USA, 1982.